Chapter 4: RF Energy Harvesting for Implantable Devices

*In this chapter, a compact and efficient dual-band rectifier for radio frequency (RF) energy harvesting is presented. The proposed design utilizes a modified T-section comprising a parallel resonance circuit combination of LC in the shunt arm, which plays a key role in obtaining the resultant dual-band rectifier. The shunt arm provides a shift of the high-frequency point in the clockwise direction on the impedance trace (Smith chart) while maintaining an insignificant shift at the lower frequency. The proposed design is verified through theoretical and simulation studies for different Schottky diodes. The circuit is optimized and fabricated to compensate for undesired parasitic effects and achieve the required rectifier performance. For validation, a dual-band rectifier working at 1.4 and 2.45 GHz is fabricated. The measured results show that with a 3.02 kΩ load, the maximum efficiencies of the rectifier achieve 65.0% and 57.0% at 1.4 and 2.45 GHz, respectively with 0 dBm input power.**

*Part of this chapter have been published: Dubey, R., Srivastava, S. K., Singh, A., & Meshram, M. K. (2023). Compact and Efficient Dual-Band Rectifier Using Modified T-Section Matching Network. *IEEE Microwave and Wireless Technology Letters*.

4.1 Introduction

Wireless power transmission (WPT) and radio-frequency energy harvesting (RF-EH) techniques have emerged as promising solutions for self-sustainable wireless devices. Thus, a growing number of low-power devices in WPT and RF-EH collect wasted energy from the ambient environment to extend the battery life [104]-[107]. The rectifier is a critical component in WPT and RF-EH systems for converting received power into usable direct current (DC) supply.

In the past, attention has been focused on single-band rectifiers [60],[77]-[78],[108] in the RF energy harvesting domain. Although single-band rectifier provides more power conversion efficiency (PCE), it suffers from narrow band characteristics. Consequently, researchers have shown increased interest in broadband [61]-[66] and dual-band rectifiers [67]-[76]. However, broad bandwidth is achieved normally at the cost of size and complexity.

The above considerations indicate that dual-band rectifier circuit provides optimum solution for WPT and RF-EH. In the recent past, L-type matching network [67], multistub networks [68], single-stage T-type network [69], half wavelength transmission line [70], three transmission line [71], stepped impedance [72], metamaterial based [73], LC network [74], and coupled line network [75] have been proposed to obtain dual-bandwidth. Most of the dual-band rectifiers used voltage-doubler [67]-[69], [73]-[76], single series [70]-[72], and single shunt [71] topologies. These rectifiers occupied large footprint and more frequency separation between two distinct bands i.e., 915 MHz and 2.45 GHz. However, it is challenging to achieve impedance matching in dual-band rectifier from small footprint when two operating frequencies are close to each other.

In this letter, a compact and efficient dual-band rectifier using a modified T-type matching

network (MTMN) is proposed for WPT applications. In order to minimize spurious passbands and a large footprint from distributed components, the modified T-type matching network is constructed using surface-mount lumped components. In this work, the single element in the shunt is replaced by a combination of a parallel inductance L and a capacitor C in the shunt in the process of impedance matching to obtain dual-band rectifier characteristics. We have initially demonstrated using simulation that the lumped-element impedance matching network can be used along with microwave Schottky diodes to achieve dual-band performance. To verify the design concept, a dual-band rectifier working in the wireless medical telemetry service (WMTS) (1.4 GHz) [77] [78] and industrial, scientific, and medical (ISM) radio band is fabricated and tested. We also successfully tested the working of digital calipers and lit an LED using RF-EH. The total rectifier circuit dimensions are 16 x 9.0 mm².

4.2 Design and Analysis of the Dual-Band Rectifier Circuit

Fig.4.1. shows the schematic of the proposed dual-band rectifier based on voltage doubler configuration to increase the output dc voltage [69]. It consists of a DC-block capacitor (C_{in}), MTMN, Schottky diodes D_1 and D_2, a DC-pass filter (C_{out}) and a resistive load (R_L). The MTMN consists of four lumped elements L_1, L_2, L_3, and C_3. The inductor L_1 is directly coupled to the dc blocking capacitance C_{in} and a combination of parallel L_3 C_3 network in the shunt arm. Further, the circuit includes a third inductor L_2 which is coupled between the parallel resonator circuit and the feeder.

The optimum resistive load R_L should be first found for the selected maximum power conversion efficiency rectifying device, using a source-pull simulation. The targeted working frequencies are f_1 (1.4 GHz) and f_2 (2.45 GHz) for fixed input power level P_{in} of 0 dBm. Table 4.1 lists the optimum resistive load R_L for four different Schottky diodes.

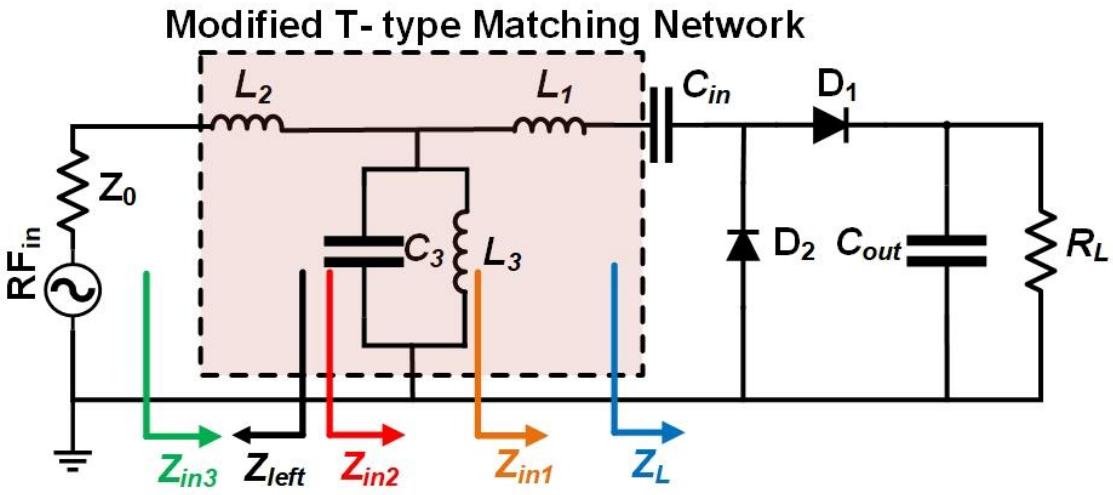

Fig. 4.1: Schematic of the proposed dual-band rectifier.

Fig. 4.2 (a) shows the load impedance Z_L at targeted frequencies for 0 dBm input power. Z_L represents the load impedance for the impedance matching network, which is frequency-dependent due to the nonlinearity of the rectifying diode and parasitic components.

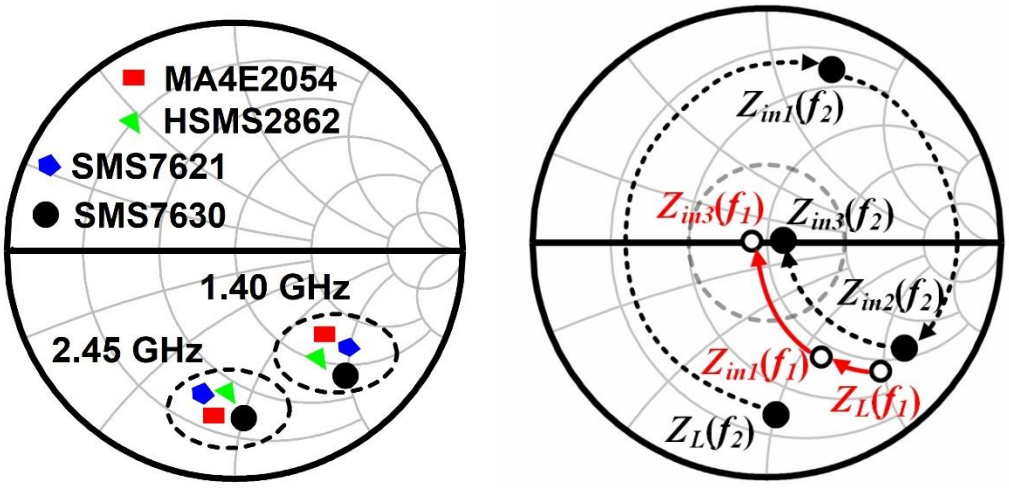

(a) (b)

Fig. 4.2: (a) Load impedance. **(b)** Design principle of the input matching network at 0 dBm input power.

4.2.1 Design and analysis of the dual-band matching network

Fig. 4.2(b). shows the design principle of the impedance matching network of the dual-band rectifier. Generally, the load impedance Z_L is frequency-dependent. Thus, it can be

denoted as R_1+jX_1 at f_1 and R_2+jX_2 at f_2. It can be seen that the load impedance has a large capacitance at targeted frequencies. To achieve the desired 50 Ω input impedance for proper matching, following steps are performed.

*Step*1. The series inductor L_1 transformed Z_L to Z_{in1}, such that $Z_{in1}\big|_{f_2} = Z_L^*\big|_{f_2}$. The reactance increases more at the f_2 than at f_1 because the increase of reactance is proportional to the frequency.

*Step*2. A tank circuit (combination of L_3 and C_3) in the shunt arm added which is coupled to L_1 such that, $\mathrm{Img}(Z_{in1})\big|_{f_1} = \mathrm{Img}(Z_{in2})\big|_{f_2}$. The resonance frequency of tank circuit selectively chosen at lower frequency f_1, hence no movement at low-frequency on the trace.

*Step*3. Finally, an inductor L_2 is inserted in series with the circuit on the input side which cancel the imaginary part of Z_{in2} , thus transforming of Z_{in2} to Z_{in3}.

The lumped components of the matching network in Fig.4.1. are estimated using equations (1)-(4) given below, which are derived using the conditions given in steps (1) -(3).

$$L_1 = \frac{-2X_2}{\omega_2} \tag{4.1}$$

$$L_2 = \sqrt{\left(\frac{Z_0}{R_1}\right)[R_1^2 + \alpha^2] - Z_0^2} \tag{4.2}$$

$$\mathrm{L_3} = \left(\frac{1}{\omega_1^2}\right)\left(\frac{\beta}{\frac{\alpha}{R_1^2+\alpha^2}+\frac{X_2}{R_2^2+X_2^2}}\right) \tag{4.3}$$

$$\mathrm{C_3} = \frac{\left(\frac{\alpha}{R_1^2+\alpha^2}+\frac{X_2}{R_2^2+X_2^2}\right)}{\beta} \tag{4.4}$$

where, $\alpha = X_2 - 2X_1\left(\frac{\omega_1}{\omega_2}\right)$ and $\beta = \omega_2\left(1 - \left(\frac{\omega_1}{\omega_2}\right)^2\right)$

The lumped component values are obtained using the aforementioned design formulas. The lumped component values for four different Schottky diodes are given in Table 4.1. To

verify the working of proposed matching network and design principle, circuit model as shown in Fig.4.1. is simulated in NI/AWR software and reflection coefficient is plotted in Fig. 4.3. for different Schottky diodes. It is observed that the load impedance is properly matched with the rectifier input impedance.

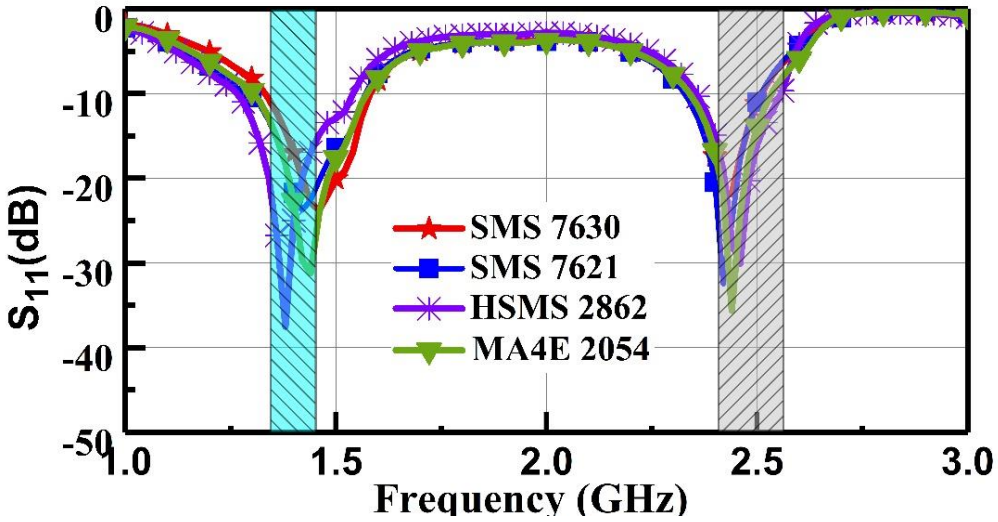

Fig. 4.3: Simulated S_{11} versus frequency for dual-band rectifier

Table 4.1: Lumped component values for different schottky diode

Model	L_1 (nH)	L_2 (nH)	L_3 (nH)	C_3 (pF)	R_L^* (kΩ)
SMS 7630	10.86	7.56	7.07	1.82	3.25
HSMS 2862	8.91	6.33	6.88	1.96	1.78
SMS 7621	10.61	6.33	7.4	1.84	1.8
MA4E 2054	10.31	6.03	7.18	1.92	1.82

*Optimum value of load resistance

4.2.2 Final design of rectifier

In order to access the impact of substrate losses, microstrip interconnection, discontinuities and the performance of the lumped components model, final circuit is designed using co-simulation method. The microstrip interconnections and discontinuities are characterized

using the full-wave simulation software (HFSS), and the effect of these parameters lumped component SPICE model parameters which are iteratively optimized using NI/AWR software. The package parasitics of Skyworks SMS7630-05LF Schottky diode is considered in the design process [78]. The details of optimized surface-mount device (SMD) components are listed in Table 4.2.

Table 4.2: Optimized surface mount devices

Components Name	Symbol	Values (kΩ, nH, pF)	Mfg.	Component no.
Inductors	L_1, L_2, L_3	9.2, 6.5, 5.8	Murata	LQG15HS
Capacitors	C_3, C_{in}, C_{out}	0.8, 100, 100	Murata	GJM1555C
Load Resistor	R_L	3.02	Vishay	CRCW0402

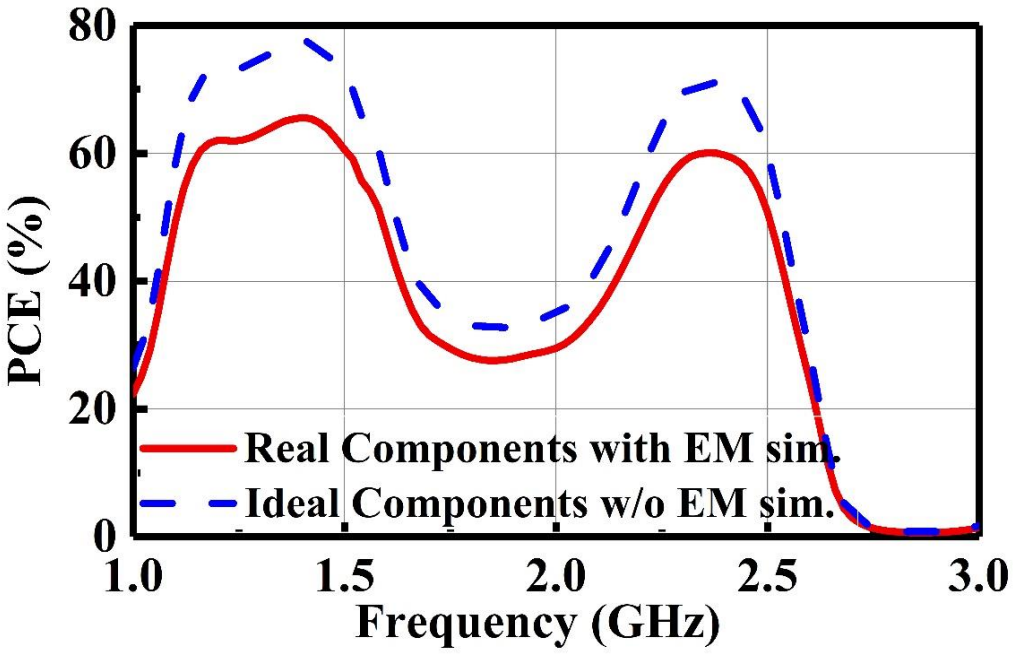

Fig. 4.4: Simulated power conversion efficiency with frequency.

Fig. 4.4. shows how discrete component and substrate losses affect circuit performance upon in terms of RF-dc conversion efficiency. The power conversion efficiency (PCE) is

reduced by approximately 12% for the rectifier operating under aforesaid conditions frequency bands of 1.4 and 2.45 GHz in comparison with an ideal rectifier as is expected.

4.3 Results and Discussion

To verify the design concept, the proposed dual-band rectifier is fabricated on a Taconic TLY substrate having thickness 0.4 mm, relative dielectric constant 2.75, and loss tangent 0.002 as shown in Fig.4.5(a). Considering achievable maximum efficiency of several commercial diodes for low incident power levels [92], Skyworks SMS7630-05LF Schottky diode is chosen as the rectifying device. The measurement process is as follows: microwave power applied to the rectifier circuit through Agilent make signal generator (E4447A; Agilent). A Falcon make digital multimeter (DMM50; Falcon) is used to measure the dc voltage. The rectifier conversion efficiency is computed using the measured values.

Fig.4.5 (b). shows a photograph of the digital caliper and LED lighting using the power harvesting circuit. Fig.4.6(a). shows the variations of simulated and measured $|S_{11}|$ and PCE with frequency. The rectifier is provided 0 dBm input power with the load resistance of 3.02 kΩ. The measured and simulated results are in good agreement with each other except in the higher frequency band where small deviation is observed. This may be due to the discrepancies in lumped components and diode model parameters between simulation and real-world scenarios at high frequencies. The measured $|S_{11}|$ are -23.34 and -21.19 dB at 1.40 and 2.45 GHz, respectively, while the simulated ones are -24.98 and -19.87 dB at the two frequencies of interest. The measured PCE values are more than 50% in the frequency bands 1.2-1.5 GHz and 2.4–2.51GHz, while more than 50 % PCE are obtained in simulation in the frequency bands 1.1-1.58GHz and 2.39-2.53 GHz. Both the measured and simulated results for PCE are in good agreement. The rectifier shows peak efficiency when the input power is 0 dBm for both bands using CW signals at each frequency/power. There are works on using multi-tone and other waveforms to improve the efficiency of rectifiers

beyond what is possible using CW signals. Future research could explore these alternative waveforms to potentially enhance the efficiency of the proposed rectifier design.

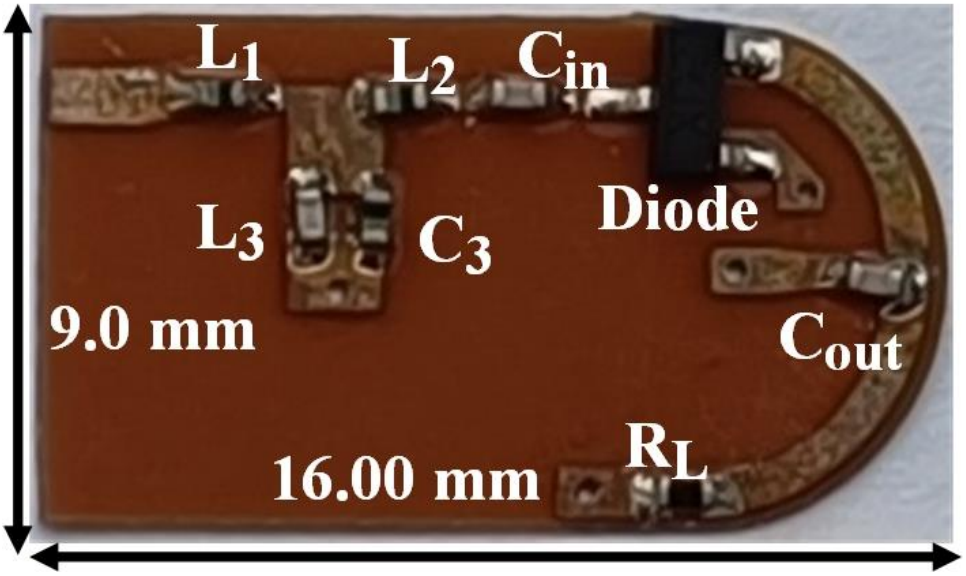

(a)

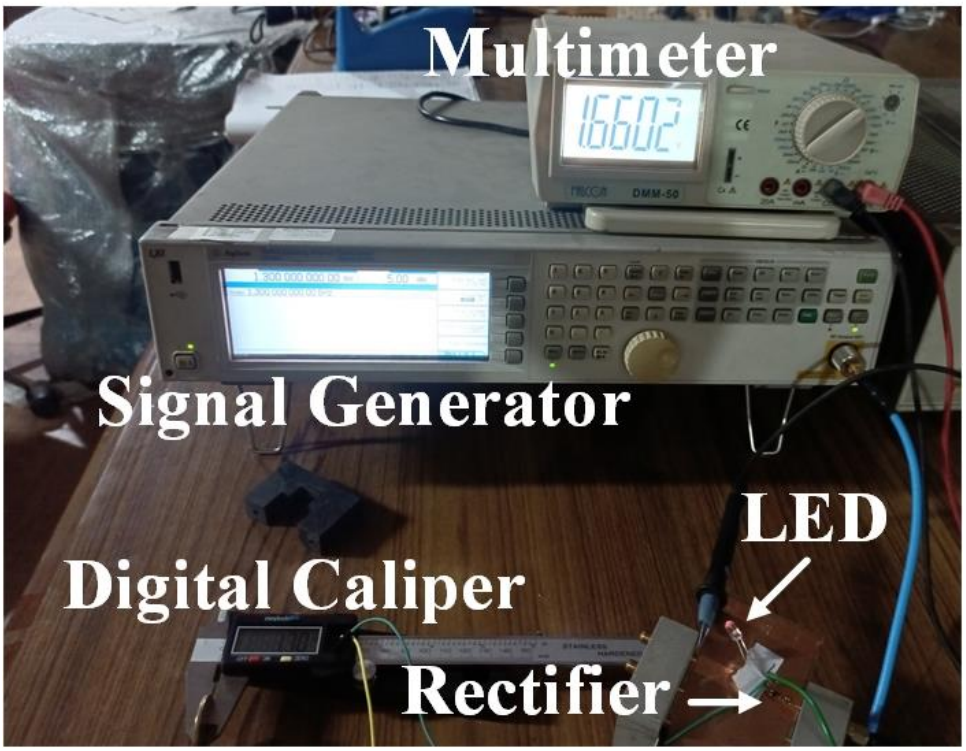

(b)

Fig. 4.5: (a) Prototype and (b) experimental validation of Proposed rectifier.

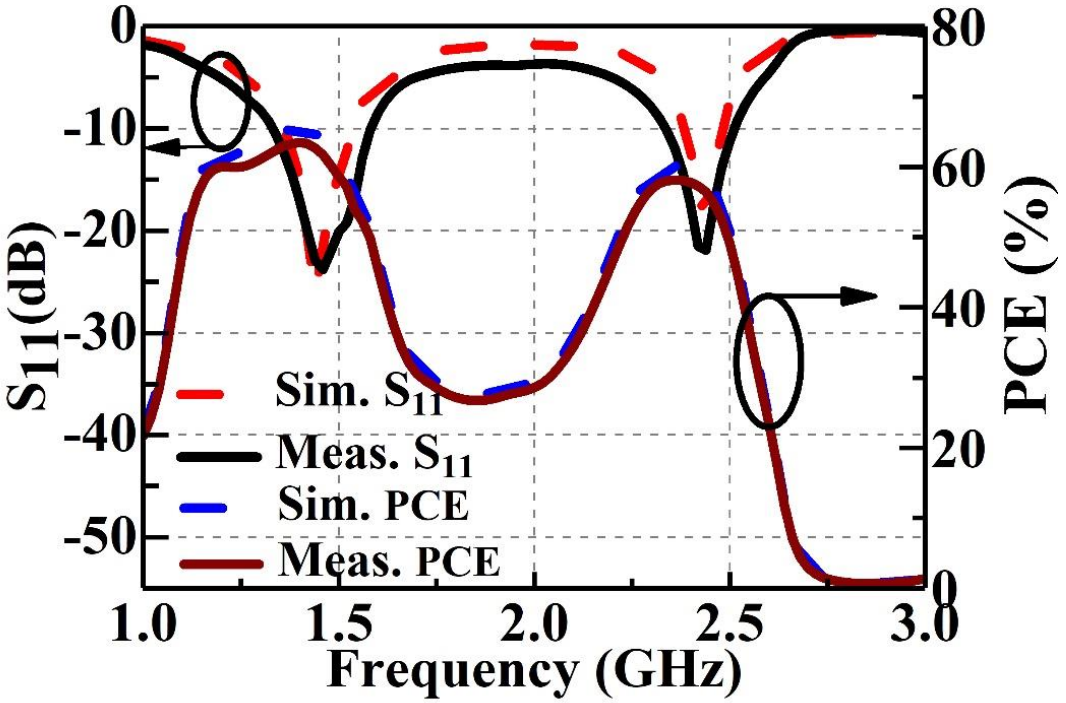

(a)

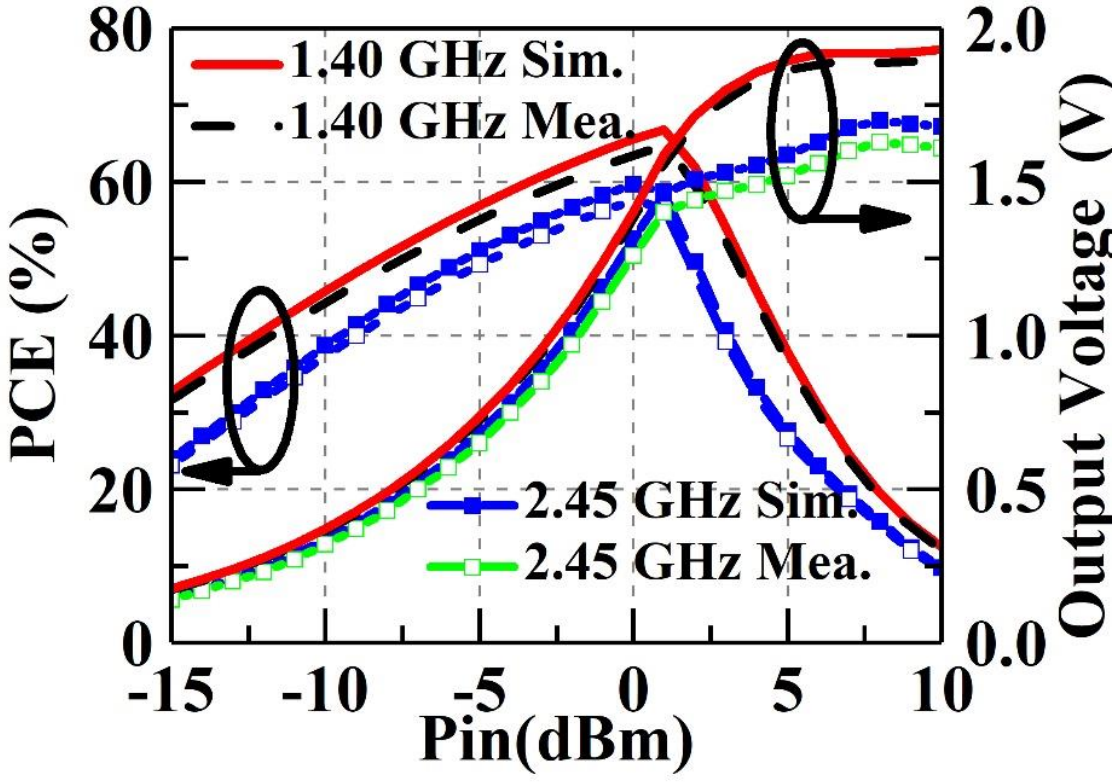

(b)

Fig. 4.6. **(a)** Reflection coefficient and power conversion efficiency with frequency and **(b)** Power conversion efficiency and output voltage with input power level.

Fig. 4.6(b). shows variations of rectifier PCE and output dc voltage versus different input power level at 1.4 and 2.45 GHz. It is observed that measured PCE values are more than 50% for input power level over the -7.5– 3.3 dBm at 1.4 GHz and -5.0–1.85 dBm at 2.45 GHz, respectively. The measured maximum efficiencies are 65% and 57% at 1.4 and 2.45 GHz, respectively, which are approximately 5% lower than the simulated ones. This difference can be attributed to factors such as component tolerances and real-world operating conditions. Despite this, a high DC output voltage is obtained by selecting the voltage doubler structure, making the rectifier suitable for powering implantable medical devices like wireless endoscopy capsules. Our design prioritizes adherence to safety regulations for maximum power density. In the previous chapter, we considered free space loss and tissue attenuation. However, for this specific design, we opted to use a power amplifier to maximize received power at the capsule, effectively bypassing the initial loss calculations. Future analyses will incorporate loss calculations for varying ranges and power requirements to further optimize the system for different scenarios. The performance of the proposed rectifier is compared with some recently published work in Table 4.3. It is observed that the proposed rectifier performs reasonably well in terms of efficiency and the overall size as compared with the relevant work in [67]-[75].

Table 4.3: Comparison between the proposed rectifier and the references

Ref.	Freq. f_1 ,f_2 (GHz)	Peak PCE Point		Diode	Size (λ_0^2)
		P_{in} (dBm)	PCE (%)		
[67]*	0.915, 2.45	28	71, 67.7	HSMS 2822	0.12x0.045
[69]*	0.915, 2.45	12	81.7,73.1	HSMS 2862	0.36x0.17
	0.915, 2.45	-1	69.2,64.1	SMS 7630	0.35x0.11
[71]*	0.915, 2.45	14	82.5, 71.8	HSMS 2860	0.14x0.08
[72]*	0.915, 2.45	9	74,73	BAT15-03W	0.06x0.04
[75]*	0.915, 2.45	30	66,58	HSMS 2822	0.18 x 0.24
	0.915, 2.45	30	60,58	HSMS 2852	0.18x0.24
This work#	**1.4, 2.45**	**0**	**65, 57**	**SMS 7630**	**0.07 x 0.04**

λ_0 : wavelength at the lowest frequency, f_2/f_1 : * 2.67, # 1.75.

4.4 Summary

In this chapter, a compact and efficient dual-band rectifier using a modified T-section matching circuit has been designed and developed to cover WMTS and ISM bands center at frequencies of 1.40 and 2.45 GHz with corresponding PCE values of 65.0 % and 57.0 %. The proposed rectifier has achieved a PCE above 50% over the input power ranges of -7.5 – 3.3 dBm and -5.0 –1.85 dBm at 1.40 and 2.45 GHz, respectively. Compared to relevant works, the proposed rectifier has the advantages of a smaller frequency ratio, reasonable efficiency, and a smaller footprint. This makes it a promising candidate as a rectifier in WPT, particularly in implantable medical devices. Building upon Chapter 4, the detailed exploration of a compact and efficient dual-band rectifier sets the stage for Chapter 5. The rectifier's commendable PCE values, smaller frequency ratio, and footprint position it as a promising candidate for Wireless Power Transfer (WPT), notably in implantable medical devices. This groundwork underpins the forthcoming investigation into a Dual-Band Dual-Sense Circularly Polarized High Gain Suspended Plate Antenna in Chapter 5, aimed at advancing bio-telemetry applications.